Identifying sources of rainfall derived infiltration and inflow using impulse response functions

Namjeong Choi[1] and Arthur Schmidt[2]

[1]US Geological Survey Southeast Region
[2]University of Illinois at Urbana-Champaign

April 28, 2020

Posted on Authorea 13 Apr 2020 — CC BY 4.0 — https://doi.org/10.22541/au.158679896.68487959 — This a preprint and has not been peer reviewed. Data may be preliminary.

Abstract

Rainfall derived infiltration and inflow (RDII) are extraneous water in a sanitary sewer system that are originated from rainfall in a surface runoff form. Most RDII enters sanitary sewer systems through illegal connections or mechanical faults, especially in aged sewer systems. In this study, the physical process of three primary RDII sources: roof downspout, sump pump, and leaky lateral, are investigated using physics-based models. These three sources represent three different flow paths: direct connection of impervious catchments, mixed flow through coarse porous media followed by a direct connection, and percolated flow through compacted soil, respectively. Due to the differences in medium and the flow paths, flow responses of these three RDII sources differ in time and magnitude, and they can be distinctly identified from each other. The typical flow response of each RDII source is represented as an Impulse Response Function (IRF) that is a flow response to a pre-specified representative rainfall computed using physics-based models. The total RDII flow hydrograph is presented as a combination of these three IRFs, and the weighting factors of each IRF is calibrated using a genetic algorithm (GA) technique in a test sewer catchment. The results may shed light on identifying the contributions of different RDII sources in a sewershed and help public water managers to understand the local RDII issues better, which in turn facilitates more effective management of a sewer system.

Introduction

Infiltration and inflow (I&I) is an urban water resources term that describes the unwanted water existing in sewer systems that are not originated from the typical sewer sources, e.g., domestic and industrial discharge. Infiltration is water seeping into the sewer pipes, preferably through broken pipe cracks and joints (Figure 1). The origin of infiltration can be surface water percolated down to the sewer pipes or groundwater with the water table above the pipe invert. Inflow is surface water entering the sewer system through direct connections from runoff catchments or cross-connections from storm sewer or combined sewer. The term rainfall derived infiltration and inflow (RDII) is a type of I&I that originates from rainfall, often in a surface runoff form.

I&I is one of the major problems affecting sewer systems in terms of flow overloading that causes sewer overflows, basement flooding, street flooding, increase in pumping costs, water pollution, and decrease in treatment efficiency in water treatment plants (Backmeyer, 1960; Field & Struzeski, 1972; Gottstein, 1976l; Lai, 2008). Based on the estimation by Petroff (1996), roughly 50% of the water entering wastewater treatment plants in the U.S. is from I&I. Depending on the age and the condition of the sewer system, the relative volume of I&I to the dry weather flow (DWF) could be ranged from 0.4 to 9 (Bishop et al., 1987; National Small Flows Clearinghouse, 1999; Ertl et al., 2002; Weiss et al., 2002; Lucas, 2003; Pecher, 2003; Jardin, 2004; Kretschmer et al., 2008; Bhaskar & Welty, 2012). For example, I&I for Baltimore City was nine times greater than the DWF, and it was also larger than the gauged streamflow from the urban watershed (Bhaskar & Welty, 2012). This indicates that I&I volume can affect the capacity of a sanitary sewer system significantly.

Various I&I estimation modeling methods have been developed since the 1980s to quantify the amount of I&I (De Bénédittis & Bertrand-Krajewski, 2005). Bishop et al. (1987) developed a simple synthetic hydrograph method for 300 study basins to estimate I&I and to evaluate flow data. Gustafsson (2000) presented a leakage model that takes account of the two-way interaction between pipes and the aquifer using MOUSE (Lindberg et al., 1989) and MIKE-SHE (DHI Software, 2007a;b). Karpf and Krebs (2004) also used the same leakage approach. The model was calibrated using a leakage factor that is a function of groundwater infiltration rate, groundwater level, the water level in the sewer pipe, and water level at the pipe surface to which the groundwater is exposed. Schulz et al. (2005) used the same modeling approach to estimate the potential benefits of sewer pipe rehabilitation with different hypothetical infiltration rates. Qiao et al. (2007) presented a groundwater infiltration model using a two-reservoir approach: one reservoir for soil storage in an unsaturated zone and another for groundwater storage in a saturated zone. The elevations of the reservoir openings determine the trigger points that initiate infiltration into sewer pipes.

One of the most common practices of estimating I&I contribution to sewer flow is the RTK method that was developed by Camp Dresser and McKee (CDM) Inc. et al. (1985). According to Lai (2008), "the RTK method is probably the most popular synthetic unit hydrograph (SUH) method" in the stormwater management field. This method uses unit hydrographs to estimate the response times associated with the effect of fast, moderate, and slow I&I by a linear convolution. A user may calibrate the model by comparing it to an observed I&I hydrograph. This SUH method is the foundation of the EPA Sanitary Sewer Overflow Analysis and Planning Toolbox, or SSOAP Toolbox (Vallabhaneni et al., 2008). EPA SWMM5 (Rossman, 2010) also adopted the RTK method. Despite its popularity, the model does not reflect the underlying physics of each I&I response, and it may leave a user with a vast number of possible solutions. Also, there is little guidance for calibrating these models and for I&I modeling in general (Allitt, 2002).

InfoWorks CS (Innovyze, 2011) is another popular stormwater modeling tool that has an option for I&I simulation. InfoWorks simulates I&I using two components: rainfall-induced infiltration, and groundwater infiltration. In the InfoWorks CS infiltration module, the percolation flow from the surface depression storage is assigned to the soil storage reservoir after a runoff occurs. When the soil reaches the percolation threshold, a proportion of this percolation flow goes to the sewer network, which represents RDII. The remainder of the percolation flow goes down to the groundwater storage reservoir. When the groundwater level reaches the sewer system invert level, groundwater infiltration occurs. The method enables engineers to model groundwater infiltration into a sewer system, but this approach lacks the representation of the full physical process. For example, according to the model assumption, groundwater infiltration occurs when the groundwater level is higher than the pipe invert elevation, not the water level in the sewer pipe. InfoWorks CS is popular because it provides an easy-to-use representation of RDII, and it is useful for operational design. However, the empirical approximations in this approach to model RDII and infiltration limit the ability to use this model to provide an understanding of the process behind I&I for a given system.

Both SWMM and InfoWorks take simple I&I estimation approaches that represent I&I with unit hydrographs or constant rates. Simplified modeling methods are labor- and cost-effective and easy to apply, but such approaches do not provide an understanding of processes and need much more calibration data for parameter estimation. Various I&I prediction methods, including the above methods, are well documented by Crawford et al. (1999), Wright et al. (2001), Vallabhaneni et al. (2007), and Lai (2008).

Often, the complexity of the system and lack of data prevents identifying the sources and origins of the RDII from happening. Though for convenience, the I&I sources are often categorized as fast, medium, and slow sources. The RTK method is a good example of categorizing I&I sources into different response times, where three triangular hydrographs represent short-term, intermediate-term, and long-term responses (Rossman, 2010).

Posted on Authorea 13 Apr 2020 — CC BY 4.0 — https://doi.org/10.22541/au.158679896.68487959 — This a preprint and has not been peer reviewed. Data may be preliminary.

In the physical world, the fast I&I source indicates a direct connection of impervious surface runoff catchments, e.g., roof downspout, connected to a sewer pipe. The slow I&I is the infiltration component of I&I that indicates flow through porous media. The medium-speed I&I falls in between the fast and slow I&I in terms of the time to peak. Walski et al. (2007) defined medium response as "more delayed and attenuated response to rainfall" or "rapid infiltration." Hodgson and Schultz (1995) used the footer drain as an example of the medium response. Nogaj and Hollenback (1981) pointed out that foundation drains and storm sumps are not highly sensitive to changes in rainfall intensity, which makes these inflow sources classified as medium-speed I&I sources.

The fast and medium sources are examples of illegal connections to sanitary sewer systems that lead surface water into sewer pipes. The standard practice of treating the runoff from impervious areas is to "drain to light" or drain to a gravity flow—a ditch, a storm sewer, or an overland flow surface, ideally with permeable soil. In case the storm sources are connected to sanitary sewer systems, the extra water becomes RDII. Compared to the fast- and medium-speed I&I sources, slow infiltration occurs when the sewer system fails to keep groundwater out of the system.

The objective of this paper is to identify three representative RDII sources and understand the hydrologic characteristics of the flow using the impulse response functions (IRFs). The model is calibrated using a genetic algorithm (GA) technique in a study area and eventually used to verify the relative predominance of each RDII source in the test community.

Posted on Authorea 13 Apr 2020 — CC BY 4.0 — https://doi.org/10.22541/au.158679896.68487959 — This a preprint and has not been peer reviewed. Data may be preliminary.

Data and Method

Three RDII sources were selected based on the type of flow paths: roof downspout, sump pump, and leaky lateral. Each flow path was characterized using physics-based models in a spatial domain of a simplified residential lot. The three RDII sources represent: flow through a direct connection from runoff catchments, flow through coarse porous media, and flow through compacted soil. These three flow paths can be simply referred to as fast, medium, and slow paths for convenience though it is ideal to differentiate them based on flow patterns and the medium that is involved in the processes.

The three IRFs are identified for the test sewershed that includes Hickory Hills, Palos Hills, and Bridgeview, Illinois (IL), where sewer system configurations and sewer flow monitoring data are available. Hickory Hills is a city in Cook County, IL, with a size of 7.33 km2 and a population of 14,049. The areal size of Palos Hills and Bridgeview, IL is 11.12 km2, and 10.75 km2, respectively, and the population of the cities is 17,484 and 16,446, respectively (U.S. Census Bureau, 2010).

2.1 Physics-based models

2.1.1 Roof connection model

The roof connection model consists of a sloped roof area, flat gutter, and vertical downspout. The roof area receives rainfall and conveys the flow to the rain gutter by gravity. The rain gutter is connected to a downspout(s) to transport flow to a drainage system. When the downspout is connected to a sewer system, it becomes RDII.

The flow from the roof is calculated using the one-dimensional kinematic wave model for rainfall-runoff. Two governing equations describe the rainfall-runoff process when using kinematic wave theory: one-dimensional continuity equation for unit width of sheet flow, and Manning's equation as a momentum equation for one-dimensional steady uniform flow per unit width. The one-dimensional continuity equation is as follows:

$\frac{\partial h}{\partial t} + \frac{\partial q}{\partial x} = I(1)$

where h = water depth [L], t = time [T], q= flow rate per unit width [L^2/T], x = distance in down slope (measured from upstream end of plane) [L],I = rainfall intensity [L/T].

Manning's equation can be used as a momentum equation for one-dimensional steady uniform flow per unit width as following.

$q = \frac{1.49}{n} S_0^{\frac{1}{2}} h^{\frac{5}{3}}$ (2)

where n = Manning's roughness coefficient,$S_{\ 0}$ = bottom slope.

The equation (1) and (2) can be expressed as one equation.

$\frac{\partial q}{\partial x} + \alpha\beta q^{\beta-1} \frac{\partial q}{\partial t} = I(3)$

where$\alpha = \left(\frac{1.49}{n} S_0^{\frac{1}{2}}\right)^{-\beta}$ and $\beta = 3/5$, which is the governing equation of kinematic wave model with q as only dependent variable.

The gutter is treated as a simple bucket. The outlet of downspout is treated as a weir or orifice depending on the flow condition. The gutter is modeled using the standard level-pool routing method (Chow et al., 1988). Level-pool routing is a lumped flow routing method that is suitable for a case with a horizontal water surface in the storage unit. The storage is a function of its water surface elevation. By using the stage-storage relation of the rain gutter and the stage-discharge relation of the downspout, this equation can be solved. Stage-discharge relations of the rain gutter-outlet are derived using an orifice and a weir equation.

Posted on Authorea 13 Apr 2020 — CC BY 4.0 — https://doi.org/10.22541/au.158679896.68487959 — This a preprint and has not been peer reviewed. Data may be preliminary.

2.1.2 Sump pump connection model

To derive the IRF from a sump pump, the commercial software MIKE-SHE (DHI Software, 2007a;b) is used to model flow to the sump in the single residential lot. MIKE-SHE is a spatially distributed hydrologic model that simulates surface water flow and groundwater flow in the three-dimensional gridded form. The one-dimensional gravity flow equation in MIKE-SHE is selected as the unsaturated zone equation. The gravity flow equation is a simplified version of the Richards equation, which ignores the pressure head term. The vertical driving force is entirely due to gravity. By selecting the gravity flow module, the dynamics owing to capillarity in the unsaturated zone are ignored. This is typically a valid assumption for coarse soils, and drainage trench around a house is usually filled with coarse materials. This is suitable to calculate the recharge rate of groundwater and faster and more stable than the Richards equation (Graham & Butts, 2005). The governing equation for the Richards equation is presented as follows.

$h = z + \psi$ (4)

Then the gravity equation drops the pressure term.

$h = z$ (5)

where h is hydraulic head [L], z is gravitational head [L], and ψ is pressure head [L].

The vertical gradient of the hydraulic head is the driving force to transport water. Thus, for the Richards equation,

$h = \frac{\partial h}{\partial z}$ (6)

and for the gravity equation,

$h = \frac{\partial h}{\partial z} = 1$ (7)

The volumetric flux that is obtained from Darcy's law for the gravity equation is

$q = -K\left(\theta\right) \frac{\partial h}{\partial z} = -K\left(\theta\right)(8)$

where $K\ (\vartheta\ )$ is unsaturated hydraulic conductivity [L^3/T].

For incompressible soil matrix and soil water with constant density, the continuity equation is:

$\frac{\partial \theta}{\partial t} = -\frac{\partial q}{\partial z} - S\left(z\right)(9)$

where ϑ is volumetric soil moisture [L^2] and S is root extraction sink term [L^2/T]. The sum of root extraction over the entire root zone depth is equal to the total actual evapotranspiration. Direct soil evaporation is computed only in the first node below the surface.

Substituting equation (18) onto equation (19), the following expression is derived.

$\frac{\partial \theta}{\partial t} = -\frac{\partial K(\theta)}{\partial z} - S\,(z)$(10)

This can be also expressed using the soil water capacity,$C = \frac{\partial \theta}{\partial \psi}$

$C\frac{\partial \psi}{\partial t} = \frac{\partial K(\theta)}{\partial z} - S\,(z)$(11)

This is called the gravity equation. This equation is used to calculate the unsaturated zone flow into a sump pump, which is used to derive the sump pump IRF.

The drainage trench around the house enables surface water to percolate down to the bottom of the building then feeds into the sump pump. In MIKE-SHE, sink cells are placed under the building to mimic the sump pump behavior and extract the water from the foundation. Unsaturated zone flow at the foundation level of the drainage trench area is interpreted as the total sump pump flow from the house. When the outlet of this sump pump is connected to a sewer system, this becomes I&I.

The size of the computational domain of the sump pump model is 50 meter (m) lengthwise and 26 m widthwise. The cell size is 0.33 m x 0.33 m; thus, a total of 150 $\times$ 78 or 11,700 cells in total were created. The vertical cell height is 0.2 m. The vegetation was assumed as uniform grass with Leaf Area Index 5 and Root Depth 100 mm. The horizontal width of the drainage trench is assumed as 0.33 m, and the total number of cells in the horizontal domain is 149, which corresponds to a total 50 m length of the trench. The drainage trench goes down to the base level of the house, 4 m below the surface where the sump is located.

Three soil types are employed in the sump pump model: ambient soil, impermeable soil, and extremely permeable soil. The hydraulic conductivity of the ambient soil is calculated as the average hydraulic conductivity of soil in Hickory Hills, IL,$K_{\text{ambient}} = 2.19 \cdot 10^{-7}$ meter per second (m/s; Natural Resources Conservation Service [NRCS], 2019). Hydraulic conductivity of impermeable soil is assumed as $1 \cdot 10^{-12}$ m/s and that of extremely permeable soil is assumed as $1 \cdot 10^{0}$ m/s. The hydraulic conductivity value of the extremely permeable soil, which represents backfill in the drainage trench, is within the range of the hydraulic conductivity for gravels based on Chow et al. (1988). The Averjanov model (Vogel et al., 2000) is used to simulate a hydraulic conductivity curve that shows the relationship between soil moisture and hydraulic conductivity.

$K\,(\theta) = K_S\left(\frac{\theta - \theta_r}{\theta_S - \theta_r}\right)^m$(12)

where K_s is saturated hydraulic conductivity [L/T], ϑ_Σ is saturated water content [L^3L^{-3}],ϑ_ρ is residual water content [L^3L^{-3}], and m is an empirical constant. Following values are used for the sump pump connection model: saturated moisture content $\vartheta_\Sigma = 0.38$, residual moisture content $\vartheta_\rho = 0.01$, and empirical constant $m = 13$.

For the MIKE-SHE model setting, the Van Genuchten model (Van Genuchten, 1980) is used to estimate the retention curve, which is a relationship between moisture content and pressure.

$\theta\,(\psi) = \theta_r + \frac{(\theta_S - \theta_r)}{[1 + (\alpha\psi)^n]^{1-1/n}}$(13)

where $\vartheta\,(\psi\,)$ is the water retention curve [L^3L^{-3}], ψ is suction pressure [L], a is an empirical constant as the inverse of the air entry suction ($a > 0$) [L^{-1}], and n is a measure of the pore-size distribution ($n > 1$). Following values are used for the sump pump connection model: inverse of air entry suction $a = 0.067$, and pore-size distribution $n = 1.446$.

Bulk density of ambient soil and extremely permeable soil is assumed as 1,700 kilograms per cubic meter (kg/m^3) and that of impermeable soil is assumed as 1,600 kg/m^3. Manning'sn values for overland flow computation for each surface type are estimated as 0.013, 0.025, and 0.030 for concrete side walk, asphalt shingle

Posted on Authorea 13 Apr 2020 — CC BY 4.0 — https://doi.org/10.22541/au.158679896.68487959 — This a preprint and has not been peer reviewed. Data may be preliminary.

rooftop, and grassed yard, respectively (Chow, 1959). Evapotranspiration rate is set as 2.76 millimeters per day (mm/d) which is a suggested value in the Chicago area according to Grimmond and Oke (1999).

2.1.3 Leaky sewer lateral model

Similar to the sump pump model, the leaky sewer lateral model is developed using MIKE-SHE. f

Input data

Rainfall data were obtained from the Illinois State Water Survey (ISWS) by averaging rainfall data from four nearby ISWS rain gages: G11, G12, G16, and G17 (Illinois State Water Survey, 2019). The sewer flow data were collected by the U.S. Geological Survey (USGS) at 17 monitoring locations in the spring and summer of 2009. Based on the data quality and the length, the site located on 104th Street and east of Terry Drive in a maintenance hole was selected for this study. This location receives sanitary sewer flow from Hickory Hills, Palos Hills, and Bridgeview, IL.

Both rainfall records and the sewer monitoring records are presented in Figure 2 in the period of April 17, 2009–August 3, 2009. The base flow shows the daily fluctuation of dry weather flow except when storm event occurs high flow peaks are observed, which tend to sync in time with the arrivals of rainfall peaks.

In order to only focus on the RDII portion of the sewer record, dry weather flow (DWF) needs to be estimated and separated from the sewer record. The average DWF was estimated using the DWF estimation component in Special Contributing Area Loading Program (SCALP), which is developed by Hydrocomp, Inc. (Hydrocomp 1979). SCALP is a flow routing model mainly developed for use in the Chicago area. DWF is determined on a per capita basis and distributed in time by coefficients: average DWF loading, monthly pattern, daily pattern, and hourly pattern using the following equation (Espey et al., 2009; Miller & Schmidt, 2010).

DWF = average DWF loading x monthly pattern x daily pattern x hourly pattern (14)

These DWF coefficients are estimated using data from a 14-day dry period from July 17, 2009, to July 31, 2009. The 14 days of DWF are averaged, and the set of best DWF coefficients is derived by adjusting each value until the best fit to the average DWF was achieved. Nash-Sutcliffe model efficiency coefficient is used to find the best fit (Nash & Sutcliffe, 1970).

The monthly pattern is the pattern describing the variability among months within a year. The monthly pattern values are all set to one throughout the year due to insufficient data to define them. The daily pattern describes the variability among days within a week, and the hourly pattern describes the variability among the hours of the day. The average DWF loading is calculated as 0.12 m^3/s (4.40 ft^3/s). The daily pattern shows that DWF is greater during weekends than on weekdays. The hourly pattern shows two peaks during a day: in mornings and evenings, and minimum DWF at 4 am.

2.3. Impulse Response Function derivation

A representative rainfall was introduced as model input, and three IRFs from the three physics-based modes were derived. Based on the rainfall record in Hickory Hills, IL, a total of 702 mm of rainfall was recorded from January 1 through July 31, 2009. Seventeen distinct storm events were identified manually during this period; hence the average rainfall volume for a single event was assumed as 41 mm (as 702 mm divided by 17). The maximum rainfall intensity during the same period is 14 mm/hr. Three hours of 14 mm/hr of rainfall produces a total of 42 mm of rainfall volume. Therefore, 3-hour 14-mm/hr uniform precipitation is selected as a representative rainfall. The representative uniform rainfall was used as an input of the three physics-based models to derive the IRF of each RDII process described in the models.

The representative rainfall can be used directly for the roof connection model because the antecedent moisture condition has a minimal effect on the flow response of the roof runoff. However, it cannot be used directly for

Posted on Authorea 13 Apr 2020 — CC BY 4.0 — https://doi.org/10.22541/au.158679896.68487959 — This a preprint and has not been peer reviewed. Data may be preliminary.

the gravity flow models that are used to derive the sump pump IRF and leaky lateral IRF. Infiltration and runoff processes are affected by ground conditions, e.g., land cover, land use, soil type, vegetation, seasonality, antecedent moisture condition. In order to eliminate the variability of ground conditions, the representative rainfall was added to the actual rainfall hyetograph at random times, and the resulting RDII hydrograph was subtracted by the RDII hydrograph resulting from the unaltered rainfall record. The representative rainfall was added to the actual rainfall hyetograph at ten randomly selected times between June 1 and January 31, 2009, and the IRF was calculated by averaging the individual IRF, which is the difference between the hydrographs resulting from the altered and unaltered rainfall hyetographs.

Three IRFs derived from the roof downspout, sump pump, and leaky lateral models using the representative rainfall are presented in Figure 3. The flow discharge units are normalized using the contributing areas of each model so that effective flowrates can be compared among the models. The peak values of each IRF are 0.0942, 0.0427, and 0.00902 $m^3/day/m^2$ for the roof downspout, sump pump, and leaky lateral models, respectively. By integrating the flow over time, the resulting RDII volume per unit contributing area values are 0.0118, 0.0319, and 0.0842 m (m^3/m^2). The result indicates that the roof IRF sports the shortest response time, although the total RDII volume per unit area is the smallest. At the same time, the leaky lateral IRF shows the longest response time with the largest volume per unit area. The total volume of each IRF is 2.89, 1.54, and 1.63 m^3, However, the values are not good indicators of showing the impact of each RDII source as the total volume is dependent on the size and the condition of each model domain. The order of total response time for each IRF was hours, days, and weeks for the roof downspout, sump pump, and leaky lateral, respectively.

To understand the long-term behavior of the three IRFs, each IRF is weighted based on the actual rainfall intensity record in the period of April 17–July 16, 2009. The total rainfall depth in this period was 372 mm, and the peak precipitation rate was 13 mm/hr. Based on the assumption such that resulting RDII hydrographs from each source are proportional to the rainfall, three independent hydrographs were created for the same time period. Then each hydrograph was divided by the effective contributing area to compare the net RDII volume. Figure 4 indicates the flow duration curves of the three RDII responses for the time period. The roof connection response presented in the solid black line shows a steep curve, which indicates a greater amount of RDII for a short period of time. This displays strong evidence that the flow is stormwater driven. The leaky lateral response, which is presented in a solid grey line, shows a flatter curve. This indicates that the leaky lateral IRF displays a longer flow duration than the roof IRF due to the delayed percolation through porous media. The sump pump IRF in the black dashed line falls between the roof IRF and the leaky lateral IRF. The sump pump flow path also involves flow through a porous media, but it is faster than the leaky lateral flow path as the travel distance of surface water in the sump pump model is shorter than that of the leaky lateral model, and the medium has a larger hydraulic conductivity. The shapes of the three IRFs are easily distinguishable from one another, which in turn makes them suitable as building blocks of an RDII hydrograph.

Results

A genetic algorithm (GA) is used to optimize the three scaling factors for the RDII impulse response functions (IRFs). The same method was used to calibrate the total sewer flow simulated by the SWMM RTK method for comparison. The efficiency of both RDII estimation methods is compared using the modified Nash-Sutcliffe coefficient.

$$E_j = 1 - \frac{\sum_{t=1}^{T} W_{t,j}(Q_0^t - Q_m^t)^2}{\sum_{t=1}^{T} W_{t,j}(Q_0^t - Q_0)^2} (15)$$

where Q_0^t is observed discharge at time t [T],Q_m^t is modeled discharge at time t[L^3/T], and Q_0 is the average of observed discharge [L^3/T]. The coefficient ranges from -[?] to 1 and $E = 1$ corresponds to a perfect match between the observed discharge and the modeled discharge.j is a weighting factor (j = 1, 2, and 3).W_j is

Posted on Authorea 13 Apr 2020 — CC BY 4.0 — https://doi.org/10.22541/au.158679896.68487959 — This a preprint and has not been peer reviewed. Data may be preliminary.

a weighting factor with the index j= 1 is applied to low flows, j = 2 is applied to medium flows, and j = 3 is applied to peak flow values. In the conventional Nash-Sutcliffe method, all three weighting factors are identical ($W_1 = W_2 = W_3$). In this study, weighting factors are adjusted so that the larger RDII peaks are emphasized. This modified Nash-Sutcliffe method is suitable as RDII only occurs during storm events.

The calibration period was from May 9, 2009, to June 7, 2009, and the validation period was from June 9, 2009, to July 8, 2009. The IRF method has three parameters to calibrate: roof connection scaling factor (R), sump pump connection scaling factor (S), and leaky lateral scaling factor (L). The RTK method has nine parameters to calibrate: R1, R2, R3, T1, T2, T3, K1, K2, and K3. R is a ratio of I&I discharge volume to the rainfall volume: R1 is for a fast inflow element, while R2 and R3 represent slower infiltration elements. T is the time to peak in each hydrograph (typically expressed in hours), and K is the ratio of time of recession to the time to peak.

For the GA optimization conditions, the size of the population was set as 100, and the maximum number of generations was set as 300 for both models approaches. Value 0.95 is selected as the probability of crossover for both IRF and RTK calibration. The probability of mutation is set as 0.06.

The calibrated parameter solutions for the IRF and RTK methods are presented in Table 1. The Nash-Sutcliffe model efficiency coefficient of the IRF solution is 0.534 in the calibration period and 0.560 in the validation period. The modified Nash-Sutcliffe coefficients for the IRF solution were 0.892 for the calibration period and 0.866 for the validation period when the Nash-Sutcliffe weighting factors were set as $W_1 = 3$ for $Q >$ 90-th percentile, $W_2 = 2$ for 80- $< Q <$ 90-th percentile, $W_3 = 1$ for $Q <$ 80-th percentile. Assigning larger weighting factors for high flows improved the model fit significantly. The Nash-Sutcliffe coefficient of the best RTK solution was 0.848 in the calibration period and 0.795 in the validation period.

Though the model fitness was improved by using the modified Nash-Sutcliffe method, model efficiency based on the RTK method was higher since the RTK method has three times more parameters to adjust, nine instead of three parameters. However, in the validation period, model efficiency was increased for the IRF solution while it was decreased for the RTK solution. This may imply the pitfall of the RTK method that the method is not consistent and may not be very robust.

The optimal solution of the IRF scaling factors using the GA is: R = 3,359 for roof, S = 22,653 for sump pump, and L = 19,985 for lateral. These values can be interpreted as the RDII volume contribution of each RDII source (Table 1). Contributing flow volume of each RDII source is derived by multiplying the per-unit-area flow volume of IRFs and the IRF weighting coefficients (Table 2). Then the contributing RDII volume from the roof, sump pump, and lateral become 9,710 m^3, 22,653 m^3, and 32,543 m^3, respectively, and they are 15%, 35%, and 50% of total estimated RDII flow volume. This simple calculation shows that the IRF result can be interpreted as the RDII volume contribution of different RDII sources, which shows the most problematic RDII contributor in the system volume-wise. These values need to be interpreted with caution as the IRF model application in this study is only one realization of a real system, and each sewershed is unique in terms of factors that contribute to RDII. However, this result can still provide insights into the RDII behavior of the system by providing the physical meaning of the solutions.

The IRF approach tends to be more robust because three parameters adjust three IRF that represent processes based on physics. Each IRF shape is defined independently using physics-based models, and the weighting parameters reflect the contribution from each of the three IRF. The IRF solutions are a unique solution, no matter how randomly the initial population was selected. In contrast, the RTK method gives different solutions every time the model runs. As an example, 30 sets of three RTK hydrograph solutions display widely variable results, as presented in Figure 5. Within the user-specified range for each hydrograph, the solution can be vastly different for each run. The Nash-Sutcliffe coefficient of the best case was 0.848, and that of the worst-case was 0.681. Depending on the user-specified ranges of each parameter, the results can vastly differ, and the performance is not guaranteed.

RTK method has many local optimal solutions, which indicates that nine coefficients are not independent. Thus the starting points or constraints of the parameters cause other parameters to adjust to obtain a local

Posted on Authorea 13 Apr 2020 — CC BY 4.0 — https://doi.org/10.22541/au.158679896.68487959 — This a preprint and has not been peer reviewed. Data may be preliminary.

optimum that behaves similarly good for calibration data. Box plots of the nine RTK parameters from the 30 model runs are presented in Figure 6. Greater variability is observed in RTK parameters for the second and third triangular hydrographs, especially the third one. This is because the model tries to adjust these parameters according to the given constraints of earlier parameters. Technically, different RTK local solutions can result in the same model fitness. Change in one hydrograph affects the other two hydrographs to change in a way to achieve the best fitness. This indicates the problem of the RTK method that physical processes are not reflected in the modeling.

Figure 7 shows the prediction of the monitored flow hydrograph using the IRF solution and the best case of the RTK solutions during the calibration period (Figure 7(a)) and the validation period (Figure 7(b)). On June 24, both methods predict flow peaks, but the peak is not observed in the monitored flow record. The flow peak might have happened in such a short period, and the flow monitor might have failed to capture the peak. Overall, the RTK method tends to follow the monitored hydrograph well, especially at the falling limbs of peaks, while IRF tends to underestimate the flow at the falling limbs.

The volume and the peak flow values for the estimated DWF, observed sewer flow, IRF model result, and RTK model result are summarized in Table 3. Flowrate 0.3 m^3/s is selected to define the beginning and the end of each storm. The observed sewer flow, IRF results, and RTK results are compared to the estimated DWF using the following equation.

$Compare\ to\ DWF = \frac{\text{Observed sewer}}{\text{Estimated DWF}} \times 100(16)$

The observed sewer flow is three to four times of DWF in volume and three to six times in peaks during the storms. Considering the monitoring location is sanitary only, a great deal of RDII exists in the area.

The IRF result and RTK result are compared to the observed sewer flow using the following equation.

$Compare\ to\ observed\ RDII = \frac{Predicted\ RDII - Observed\ RDII}{\text{Observed RDII}} \times 100(17)$

Both models underestimated the flow volume; the IRF method underestimates flow volume by 9% to 28%, and the RTK method underestimates flow volume by 4% to 26% compare to monitoring volume. In terms of flow peaks, the IRF method overestimated peak flowrate for May 13, May 27, and June 11 storms by 19%, 25%, and 9%, respectively. At the same time, the IRF method underestimated peak flowrate for May 15 and June 16 by 15% and 8%, respectively. RTK method overestimated peak flowrate consistently from 1% to 16%.

Residual plots of the IRF and the best RTK solutions for the calibration period and the validation period are presented in Figure 8. Residuals are the difference between the observed value of the dependent variable and the predicted value. Each data point has one residual and is defined with the following equation.

Residual = Observed value – Predicted value (18)

Residuals are plotted against the observed value in the x-axis. There are clusters of points at low flowrate, which represent tails in the hydrographs. In Figure 8(a), IRF underestimates the peaks as most of the residuals are on the positive side. These points were from the storms on May 15, 2009, and May 27, 2009. The same trend exists in the validation period, and the outliers were from the storms on June 11, 2009, and June 16, 2009 (Figure 8(b)). In the validation period, RTK also underestimated peaks as most of the high flow points are on the positive side. This means the best RTK solution for the calibration period loses efficiency in the validation period. This explains the decrease of the Nash-Sutcliffe coefficient of the RTK method in the validation period, as presented in Table 1, and supports that the RTK method is more of a curve fitting method with a limited physical meaning.

Posted on Authorea 13 Apr 2020 — CC BY 4.0 — https://doi.org/10.22541/au.158679896.68487959 — This a preprint and has not been peer reviewed. Data may be preliminary.

Conclusion

In this study, three major rainfall derived infiltration and inflow (RDII) sources: roof downspout, sump pump, and leaky lateral were identified, and the physical process of each source was modeled using physics-based models. These three sources represent three different flow paths: a direct connection of runoff catchments, coarse porous media, and compacted soil, respectively. The typical flow response of each RDII source was expressed as impulse response functions (IRFs) that indicate the flow responses to a representative rainfall. The three IRFs displayed distinctly different flow patterns. Roof connection IRF directly reflected the input rainfall in terms of flow duration. The leaky lateral IRF showed a delayed and dampened flow hydrograph as percolation through porous media being the major hydrologic process. The sump pump IRF hydrograph fell between the roof IRF and the leaky lateral IRF. The sump pump flow path also involved a flow through the porous medium, but the process was “faster” than the leaky lateral flow path. It is due to the travel distance of surface water in the sump pump model was shorter than that of the leaky lateral model, and the medium usually has a larger hydraulic conductivity. The shapes of the three IRFs were easily distinguishable from one another, which in turn made them suitable for use as building blocks of an RDII estimation model.

The RDII estimation using the three IRFs was achieved by superposing the IRFs to best fit the monitored RDII hydrograph. To reproduce the total RDII, each IRF was multiplied by weighting factors that were calculated using a genetic algorithm (GA) technique. This method was applied to a study sewershed in a suburb of Chicago, IL, where sewer flow monitoring data is available. The IRF model performance was compared to a more widely used method, RTK, to evaluate the advantages and disadvantages of using the suggested approach (Camp Dresser & McKee Inc., 1985; Rossman, 2010).

Discussion

The suggested Impulse Response Function (IRF) method was directly compared with the conventional RTK method. The RTK method displayed a better model efficiency than the IRF method. However, the RTK method being a simple curve fitting method caused the solutions to be variable each time. This might give a modeler a decent representation of the overall RDII, but each RTK parameter might not provide any physical meanings as they are not unique. The combinations of the nine RTK parameters can be vastly different depending on the level of experience that a model has for the model basin. In contrast, the IRF method presented consistent results.

The IRF method is a physics-based RDII estimation method that is combined with a synthetic hydrograph approach. The RTK method uses a simple curve fitting approach of three triangular hydrographs that represent fast, medium, and slow I&I sources. Because of its flexibility and ability to manipulate any hydrographs, the model tends to provide a decent calibration result. However, the RTK method has many local optimal solutions as nine calibratable coefficients are not independent of each other. While the RTK method displayed better model fitness than the IRF method, The IRF result showed improved model efficiency in the validation period than the calibration period, which might imply the robustness of the modeling approach of using physics-based models.

Moreover, predefining IRFs for each modeling unit can speed up the modeling process, which could help to develop a real-time RDII forecast model in the future. Running the entire physics-based model from scratch for every storm event might not be a feasible option. Thus the IRF approach might be desirable for decision making in urban drainage management.

Another benefit of using the three IRF approach is being able to identify relative contributions of different RDII sources when the model is calibrated. Weighting factors of each modeling unit may provide insights on which RDII source is most problematic in the test sewershed. In turn, this study can shed light on defining RDII based on its sources, which helps decision-makers to better understand their unique local RDII issues and facilitate more effective management of the sewer system.

Posted on Authorea 13 Apr 2020 — CC BY 4.0 — https://doi.org/10.22541/au.158679896.68487959 — This a preprint and has not been peer reviewed. Data may be preliminary.

The results of this study need to be interpreted with caution as it presents only one realization of the method in a selected sewershed. Each sewershed has unique characteristics, e.g., age and material of the sewer system, typical house configuration, drainage practices. Every system deals with different RDII challenges, and some do not even have RDII issues, especially in a newly constructed area. The value of this study is to demonstrate the possibility of modeling RDII using physics-based models that take into account hydrological processes.

Reference

Allitt, R. (2002). Rainfall, runoff and infiltration re-visited. WaPUG Spring Meeting 2002. pp.1–9.

Backmeyer, D. P. (1960). Effects of infiltration. *Water Pollution Control Federation 32* (5). pp.539–540.

Bhaskar, A. S., & Welty, C. (2012). Water balances along an urban-to-rural gradient of metropolitan Baltimore, 2001–2009.*Environmental & Engineering Geoscience* , *XVIII* (1), pp.37–50.

Bishop, W. J., Diemer, D. M., & Wallis, M. J. (1987). Regional infiltration/inflow study solves wet weather sewer problems.*Journal of Water Pollution Control Federation* , *59* (5), pp.289–293. Retrieved from http://www.jstor.org/stable/25043247?origin=JSTOR-pdf.

Carlier, J. P., Kao, C., & Ginzburg, I. (2007). Field-scale modeling of subsurface tile-drained soils using an equivalent-medium approach.*Journal of Hydrology* , *341* (1–2), pp.105–115. Retrieved from https://doi.org/10.1016/j.jhydrol.

Camp Dresser & McKee (CDM) Inc., F.E. Jordan Associates Inc., James M. Montgomery Consulting Engineers. (1985). *East Bay Infiltration/Inflow Study Manual for Cost-Effectiveness Analysis* : Oakland, CA: East Bay Municipal Utility District (EBMUD).

Chow, V. T. (1959). *Open-channel Hydraulics* . McGraw-Hill. p.680.

Chow, V. T., Maidment, D. R., & Mays, L. W. (1988). *Applied Hydrology* . New York: McGraw-Hill.

Crawford, D., Eckley, P., & Pier, E. (1999). Methods for estimating inflow and infiltration into sanitary sewers. *New applications in modeling urban water systems, Volume 7,* Conference on Stormwater and Related Water Systems Modeling; Management and Impacts. pp. 299–315. Toronto: CHI.

De Bénédittis, J. & Bertrand-Krajewski, J. L. (2005). Infiltration in sewer systems: comparison of measurement methods. *Water Science and Technology. 52* (3). pp.219–227. Retrieved from https://iwaponline.com/wst/issue/52/3.

DHI Software. (2007a). *MIKE SHE user manual volume 1: user guide*(Vol. 1).

DHI Software. (2007b). *MIKE SHE user manual volume 2: reference guide* (Vol. 2).

Espey, W.H., Melching, C.S., & Muste, M. (2009). *Lake Michigan Diversion, Report of the Sixth Technical Committee for Review of Diversion Flow Measurement and Accounting Procedures* . Prepared for the U.S. Army Corps of Engineers, Chicago District, Chicago, IL.

Ertl, T. W., Dlauhy, F., & Haberl, R. (2002). Investigations of the amount of infiltration/inflow into a sewage system. In Proceedings of the 3rd Sewer Processes and Networks International Conference. Paris, France.

Field, R., & Struzeski, E. J. (1972). Management and control of combined sewer overflows. *Water Pollution Control Federation* ,*44* (7), pp.1393–1415.

Gottstein, L. E. (1976). *Sewer system evaluation for infiltration/inflow* . Minneapolis, Minnesota.

Graham, D. N., & Butts, M. B. (2005). Flexible integrated watershed modeling with MIKE SHE. In V. P. Singh & D. K. Frevert (Eds.),*Watershed Models.* pp.245–272. CRC Press.

Grimmond, C. S. B., & Oke, T. R. (1999). Evapotranspiration rates in urban areas. In Impacts of Urban Growth on Surface Water and Groundwater Quality (Proceedings of IUGG 99 Symposium HS5). pp.235–243. Brimingham.

Posted on Authorea 13 Apr 2020 — CC BY 4.0 — https://doi.org/10.22541/au.158679896.68487959 — This a preprint and has not been peer reviewed. Data may be preliminary.

Gustafsson, L. (2000). Alternative drainage schemes for reduction of inflow/infiltration - prediction and follow-up of effects with the aid of an integrated sewer/aquifer model. In 1st International Conference on Urban Drainage via Internet. pp.21–37.

Hodgson, J.E., Ward, C.J.W., & Schultz, N.U. (1995). Sanitary sewage discharges in the city of Edmonton, Alberta, 1995 in Seminar publication: National Conference on Sanitary Sewer Overflows (SSOs) in April 24-26, 1995. Washington, DC. pp.403-413.

Hydrocomp. (1979). Chicago Sanitary and Ship Canal Hydrologic Calibration, report to the Northeastern Illinois Planning Commission, Chicago, IL, Areawide Clean Water Planning, Water Quality Evaluation.

Illinois State Water Survey. (2019). Cook County Precipitation Network: Data Collection, Data provided by the Illinois State Water Survey (ISWS) located in Champaign and Peoria, Illinois, and on the web at https://isws.illinois.edu, Retrieved from https://www.isws.illinois.edu/data/ccprecipnet/livedata.asp.

Innovyze. (2011). *InfoWorks CS technical review* .

Jardin, N. (2004). Fremdwasser – eine grundsätzliche Problembeschreibung (Extraneous water – a basic description). In Proceedings of 3rd Forum Ruhrverband. Essen, Germany.

Karpf, C., & Krebs, P. (2004). Sewers as drainage systems – quantification of groundwater infiltration. In Novatech 2004, 6th International conference on sustainable techniques and strategies in urban water managementWater Management. pp.969–975. Lyon.

Kretschmer, F., Ertl, T., & Koch, F. (2008). Discharge monitoring and determination of infiltration water in sewer systems. In 11th International Conference on Urban Drainage. pp.1–7. Edinburgh, Scotland, UK.

Lai, F. D. (2008). *Review of sewer design criteria and RDII prediction methods* . Washington, DC: EPA.

Lindberg, S., Nielsen, J. B., & Carr, R. (1989). An integrated PC-modelling system for hydraulic analysis of drainage systems. In Watercomp '89: The First Australasian Conference on Technical Computing in the Water Industry. Melbourne, Australia.

Lucas, S. (2003). *Auftreten, Ursachen und Auswirkungen hoher Fremdwasserabflüsse – eine zeitliche und räumliche nalyse (Occurence, causes and effects of high extraneous water flows)* . Universität Karlsruhe.

Miller, K., & Schmidt, A. R. (2010). *Hydraulic modeling of the Calumet interceptor network, Tunnel and Reservoir plan,* Report No.10. Urbana, IL: University of Illinois at Urbana-Champaign.

Nash, J. E., & Sutcliffe, J. V. (1970). River flow forecasting through conceptual models, Part I - a discussion of principles. *Journal of Hydrology* , *10* , pp.282–290.

Nogaj, R. J., & Hollenbeck, A. J. (1981). One technique for estimating inflow with surcharge conditions. *Journal of Water Pollution Control Federation* , *53* (4), pp.491–496.

National Small Flows Clearinghouse (NSFC). (1999). Infiltration and inflow can be costly for communities. Pipeline: Small Community Wastewater Issues Explained to the Public, Vol.10, No.2.

Pecher, K. H. (2003). Fremdwasseranfall, Schwankungen und Konsequenzen für die Abwasserbehandlung (Amount of I/I, variations and consequences). In Proceedings of 36th Essener Tagung, Gewässerschutz-Wasser-Abwasser. Aachen, Germany.

Petroff, R. G. (1996). An analysis of the root cause of sanitary sewer overflows. In Seminar Publication National Conference on Sanitary Sewer Overflows (SSOs): April 24-26, 1995, Washington D.C. pp.8–15. Cincinnati, OH: EPA.

Qiao, F., Lu, H., Derr, H. K., Wang, M., & Chen, M. (2007). A new method of predicting rainfall dependent inflow and infiltration. *Water Environment Federation.* pp.1883–1890. Retrieved from https://doi.org/10.2175/1938647077881160

Rossman, L. A. (2010). *Storm water management model user's manual version 5.0* . Cincinnati, OH.

Posted on Authorea 13 Apr 2020 — CC BY 4.0 — https://doi.org/10.22541/au.158679896.68487959 — This a preprint and has not been peer reviewed. Data may be preliminary.

Sargent, S. W. (2011). How often will sewage spill?: Stochastic analysis & design of a waste-water system with large RDII components. *Water New Zealand.* pp.1–28.

Schulz, N., Baur, R., & Krebs, P. (2005). Integrated modelling for the evaluation of infiltration effects. *Water Science and Technology* ,*52* (5), pp.215–223. Retrieved from http://www.ncbi.nlm.nih.gov/pubmed/16248198.

Natural Resources Conservation Service, United States Department of Agriculture. (2019). U.S. General Soil Map (STATSGO2). Retrieved from https://sdmdataaccess.sc.egov.usda.gov.

U.S. Census Bureau. (2010). Profile of General Population and Housing characteristics: 2010 Demographic Profile Data (DP-1): Hickory Hills city, Illinois, American Factfinder. Retrieved from http://factfinder.census.gov/faces/tablese

Vallabhaneni, S., Chan, C. C., & Burgess, E. H. (2007). *Computer tools for sanitary sewer system capacity analysis and planning* . Cincinnati, OH.

Van Genuchten, M. T. (1980). A closed-form equation for predicting the hydraulic conductivity of unsaturated soils. *Soil Science Society of America* , *44* (5), pp.892–898.

Vogel, T., Van Genuchten, M. T., & Cislerova, M. (2000). Effect of the shape of the soil hydraulic functions near saturation on variably-saturated low predictions. *Advances In Water Resources* ,*24* , pp.133–144.

Walski, T. M., Barnard, T. E., Harold, E., Merritt, L. B., Walker, N., & Whitman, B. E. (2007). Wet weather wastewater flows. *Wastewater collection system modeling and design* (1st ed.). pp.203–270. Bentley Institute Press.

Weiss, G., Brombach, H., & Haller, B. (2002). Infiltration and inflow in combined sewer systems: long-term analysis. *Water Science and Technology* , *45* (7), pp.11–19. Retrieved from http://www.ncbi.nlm.nih.gov/pubmed/11989885.

Wright, L., Dent, S., Mosley, C., Kadota, P., & Djebbar, Y. (2001). Comparing rainfall dependent inflow and infiltration simulation methods. In W. James (Ed.), *Models and Applications to Urban Water Systems. Monograph 9* . pp.235–257. Ontario, Canada: CHI.

Posted on Authorea 13 Apr 2020 — CC BY 4.0 — https://doi.org/10.22541/au.158679896.68487959 — This a preprint and has not been peer reviewed. Data may be preliminary.

Tables

Table 1. IRF and RTK results with Nash-Sutcliffe coefficients for the calibration period (May 9, 2009 to June 7, 2009) and validation period (June 9, 2009 to July 8, 2009)

Method	Estimated parameters	Nash-Sutcliffe coefficient Calibration	Nash-Sutcliffe coefficient Validation
IRF	R+ = 3,359, S = 14,663, L = 19,985	0.534	0.560
IRF with modified Nash-Sutcliffe++	R = 3,359, S = 14,663, L = 19,985	0.899	0.866
RTK	R1 = 0.02, T1 = 0.338, K1 = 2 R2 = 0.0478, T2 = 1, K2 = 10 R3 = 0.123, T3 = 8.5493, K3 = 14.6686	0.848	0.795

(+R = Roof connection scaling factor, S = Sump pump connection scaling factor, L = Leakey sewer lateral scaling factor,

++Weighting factors used for the modified Nah-Sutcliffe model are $W_1 = 3$ for $Q > 90$-th percentile, $W_2 = 2$ for 80- $< Q <$ 90-th percentile, and $W_3 = 1$ for $Q < 80$-th percentile.)

Posted on Authorea 13 Apr 2020 — CC BY 4.0 — https://doi.org/10.22541/au.158679896.68487959 — This a preprint and has not been peer reviewed. Data may be preliminary.

Table 2. Contributing flow volume of three RDII sources using the IRF volume and the weighting coefficients

	Roof	Sump	Lateral
Effective contributing area (m^2)	246	48	19
Flow volume under IRF (m^3)	2.89	1.54	1.63
Flow volume per unit area (m)	0.012	0.032	0.084
IRF weighting coefficients	3,359	14,663	19,985
Total contributing volume (m^3)	9,701	22,653	32,543
Contributing volume / total RDII volume (%)	15	35	50

Table 3. Volume and peak of the DWF, estimated and observed RDII using IRF and RTK for five storm events

Storm event in 2009	Estimated DWF by flow separation	Estimated DWF by flow separation	Observed RDII	Observed RDII	Predicted RDII using IRF	Predicted RDII using IRF	Predicted RDII using RTK	Predicte RDII us RTK
	Volume+	Peak++	Volume+ Compare to DWF (by multiplication; observed/DWF)	Peak++ Compare to DWF (by multiplication; observed/DWF)	Volume+ Compare to observed RDII (in percent; [observed − predicted]/observed x 100)	Peak++ Compare to observed RDII (in percent; [observed − predicted]/observed x 100)	Volume+ Compare to observed RDII (in percent; [observed − predicted]/observed x 100)	Peak++ Compar to observed RDII (in percent [observed − predicted]/ x 100)
May 13	12.23	0.15	40.49	0.53	34.74	0.63	35.49	0.58
			3.31	3.53	-14	19	-12	9
May 15	15.16	0.17	51.03	0.74	40.8	0.63	48.8	0.84
			3.37	4.35	-20	-15	-4	14
May 27	10.77	0.15	43.36	0.83	39.47	1.04	40.77	0.96
			4.03	5.53	-9	25	-6	16
June 11	13.75	0.15	60.35	0.88	43.28	0.96	44.94	0.89
			4.39	5.87	-28	9	-26	1
June 16	19.08	0.15	77.63	0.85	56.56	0.78	59.69	0.93
			4.07	5.67	-27	-8	-23	9

(+ in 10^3 m^3, ++ in m^3/s)

Figure legends

Figure 1. Captured images of root intrusion in sewer pipes through (a) pipe cracks, and (b) pipe joints (Urbana Champaign Sanitary District, 2012)

Figure 2. Rainfall and sewer flow data: (a) rainfall record from ISWS, and (b) sewer flow data from USGS sewage monitoring site in the period of April 17–August 3, 2009

Figure 3. Impulse response functions from the roof connection, sump pump, and leaky lateral models as flow discharge per unit contributing area (Black solid line indicates the roof IRF, black dashed line indicates the sump pump IRF, and the grey solid line indicates the leaky lateral IRF.)

Figure 4. Exceedance probability of three RDII responses per unit area in log scales in the period of April 17–July 16, 2009

Figure 5. Three RTK triangular hydrographs from 30 different model runs that show inconsistency of the solutions: (a) "fast" hydrograph, (b) "medium" hydrograph, and (c) "slow" hydrograph

Figure 6. Box plots of RTK solutions that indicate interdependency of the nine parameters: R1, R2, R3, T1, T2, T3, K1, K2, and K3 (R: ratio of I&I discharge volume to the rainfall volume, T: time to peak in each hydrograph, K: ratio of time of recession to the time to peak, 1: fast inflow element, 2: medium infiltration element, and 3: slow infiltration element)

Figure 7. Calibrated IRF and the best RTK results in the (a) calibration period (May 9–June 7, 2009) and the (b) validation period (June 9–July 8, 2009)

Figure 8. Residual plots of IRF (depicted with light grey diamonds) and RTK methods (depicted with dark grey squares) for (a) calibration period and (b) validation period

Data Availability Statement

The data that support the findings of this study are available from the corresponding author, Namjeong Choi, upon reasonable request.

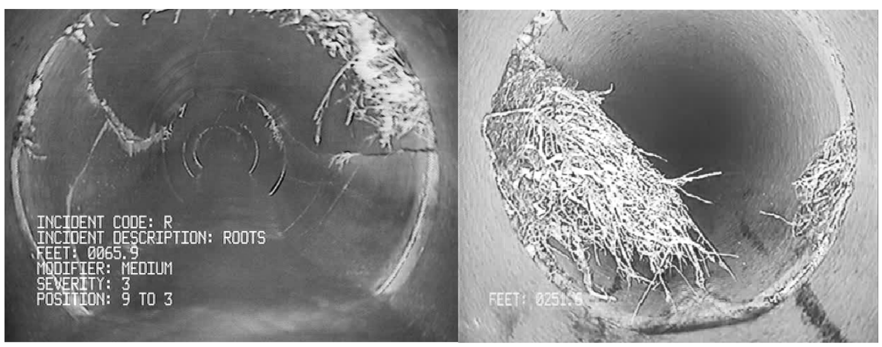

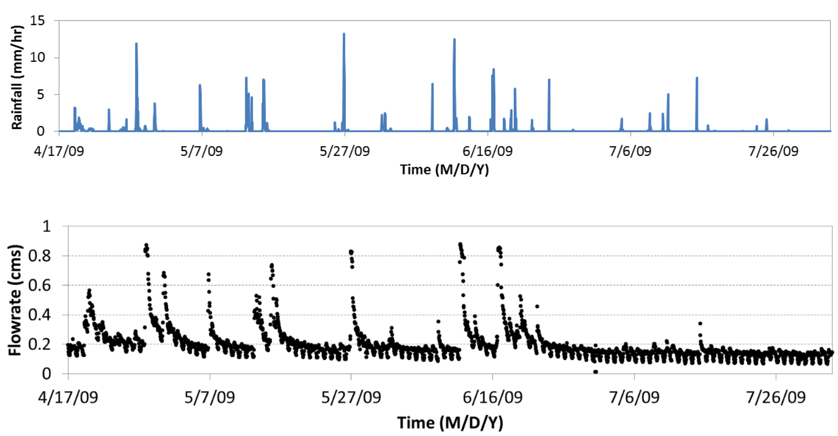

Posted on Authorea 13 Apr 2020 — CC BY 4.0 — https://doi.org/10.22541/au.158679896.68487959 — This a preprint and has not been peer reviewed. Data may be preliminary.

Posted on Authorea 13 Apr 2020 — CC BY 4.0 — https://doi.org/10.22541/au.158679896.68487959 — This a preprint and has not been peer reviewed. Data may be preliminary.

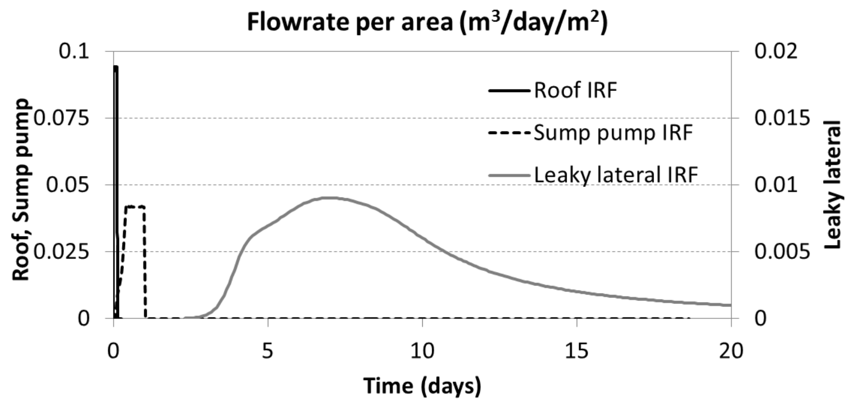

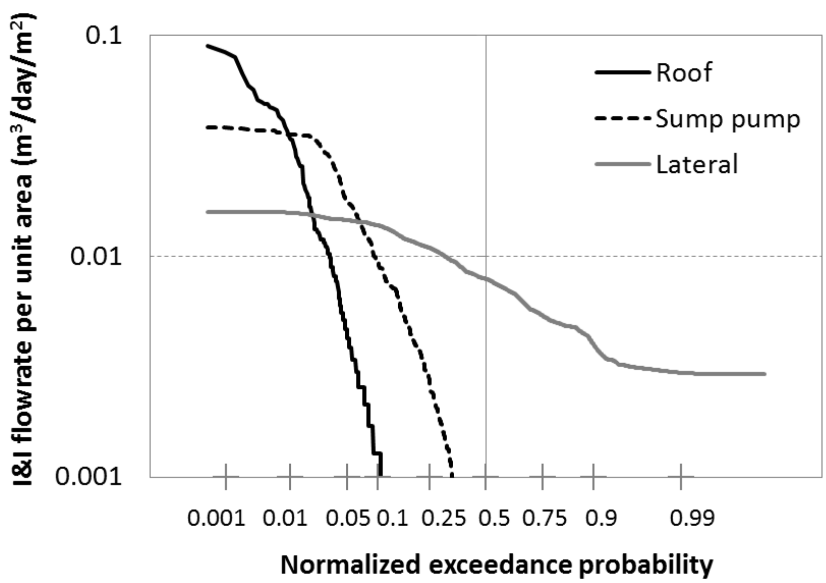

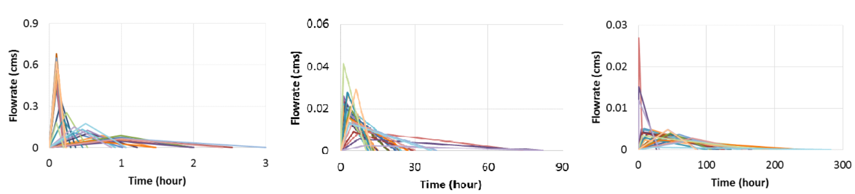

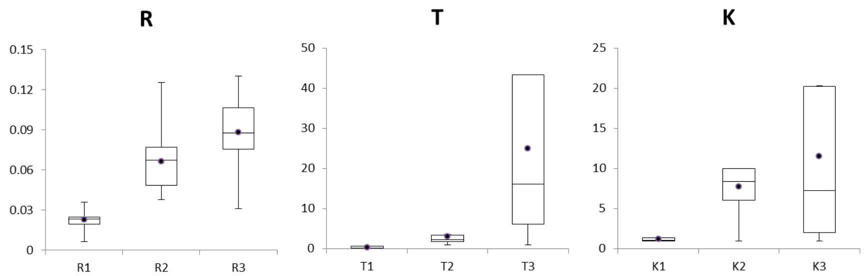

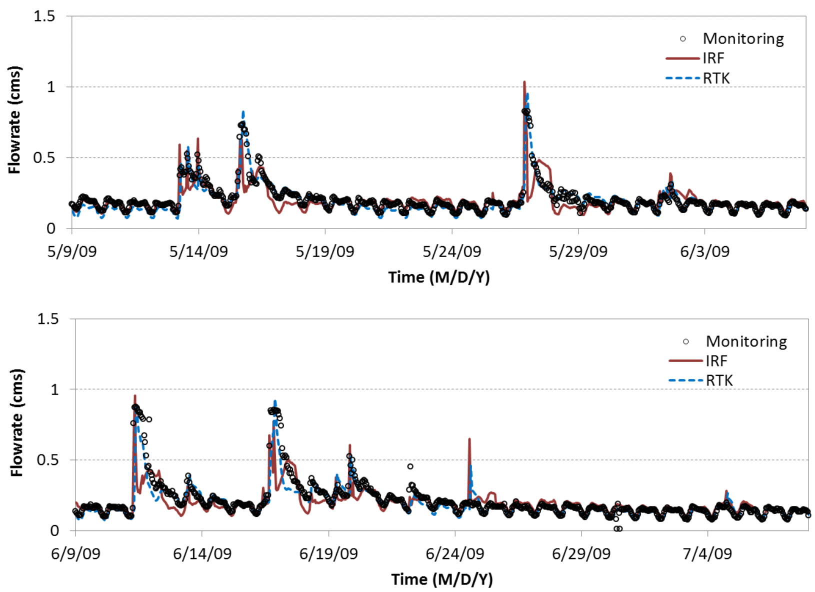

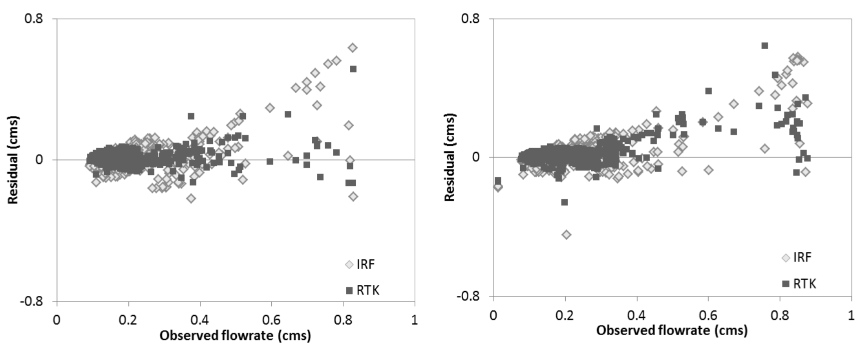

Posted on Authorea 13 Apr 2020 — CC BY 4.0 — https://doi.org/10.22541/au.158679896.68487959 — This a preprint and has not been peer reviewed. Data may be preliminary.